Planar Self-Similar Antennas for Broadband Millimeter-Wave Detectors

J. Meinke[1], P. Mauskopf[1,2], B. R. Johnson[3], D. Flanigan[3], K. Irwin[4], D. Li[5], H.-M. Cho[5], P. Day[6], J. McMahon[7], S. Doyle[8], P. A. R. Ade[8]

[1] Department of Physics, Arizona State University, Tempe, Arizona 85287, USA
[2] School of Earth and Space Exploration, Arizona State University, Tempe, Arizona 85287, USA
[3] Department of Physics, Columbia University, New York, NY 10027, USA
[4] Department of Physics, Stanford University, Stanford, CA 94305-4085, USA
[5] SLAC National Accelerator Laboratory, Menlo Park, CA 94025, USA
[6] NASA, Jet Propulsion Lab, Pasadena, CA 91109, USA
[7] Department of Physics, University of Michigan, Ann Arbor, MI 48103, USA
[8] School of Physics and Astronomy, Cardiff University, Cardiff CF243AA, UK

Introduction

Planar self-similar and self-complementary antennas are broadband, frequency-independent, and easily scalable. Impedance of opposing arms in an n-arm design can be determined with an adjusted Babinet's Principle [1]:

$$Z_{slot} Z_{metal} = \left(\frac{Z_0}{2 sin(\frac{\pi}{n})} \right)^2 \quad (1)$$

Which simplifies further by $Z_{slot} = Z_{metal}$ for self-complementary layouts.

A four-arm design places identical arms every 90°, with a similar slot/gap spaced between them. Opposing arms couple to linear polarization, so these four-arm antennas can detect both orthogonal polarizations simultaneously.

The most basic case is the bowtie design as shown in Fig. 1. The dimensions can be scaled to the desired frequency range. Our goal is the polarization detection of the Cosmic Microwave Background (CMB) in the mm-wavelengths (95/150/220 GHz bands).

Figure 1: Invariantly scalable bowtie self-similar design. The four arms (orange) are rotationally symmetric to one another and the gaps between them (self-complementary).

In-device, microstrips are placed over each arm that then jump across and down to a central cross-feed (Fig. 2). The antennas are also paired with an extended hemisphere silicon lenslet for better beam characteristics (Fig. 3). It includes a two-layer anti-reflection (AR) coating.

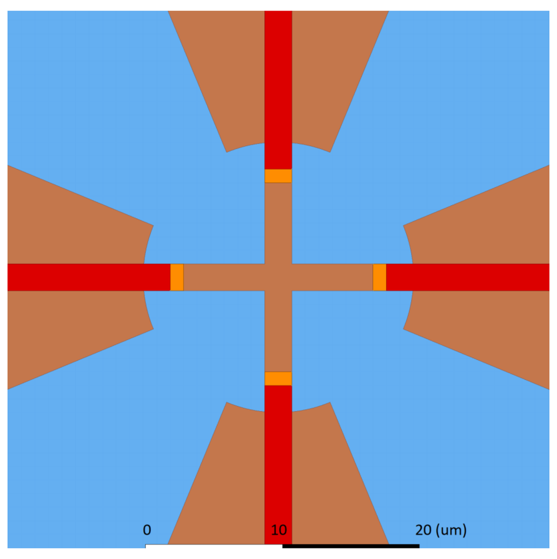

Figure 2: Close-up diagram of microstrips (red) run over basic bowtie arms, then dropping down to a central cross-feed.

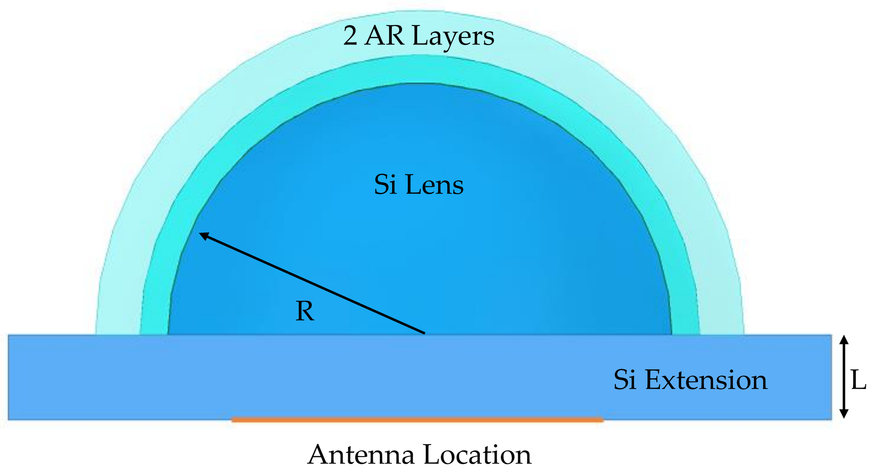

Figure 3: Silicon extended hemisphere lenslet to be placed over antenna. The beam is directed and focused forward while the AR coatings reduce reflection at the lens interface.

Designs

Figure 4: Self-complementary log-periodic (or -like) antenna designs. **A)** Sinuous log-periodic unit cell and pattern, invariantly scalable. **B)** Trapezoidal log-periodic unit cell and pattern for S=50% (unit cell midway between an S=0 triangular and S=100 rectangular shape), also invariantly scalable. **C)** Hybrid Trapezoidal (no longer log-periodic), made/chosen for capable fabrication with a 2 um microstrip.

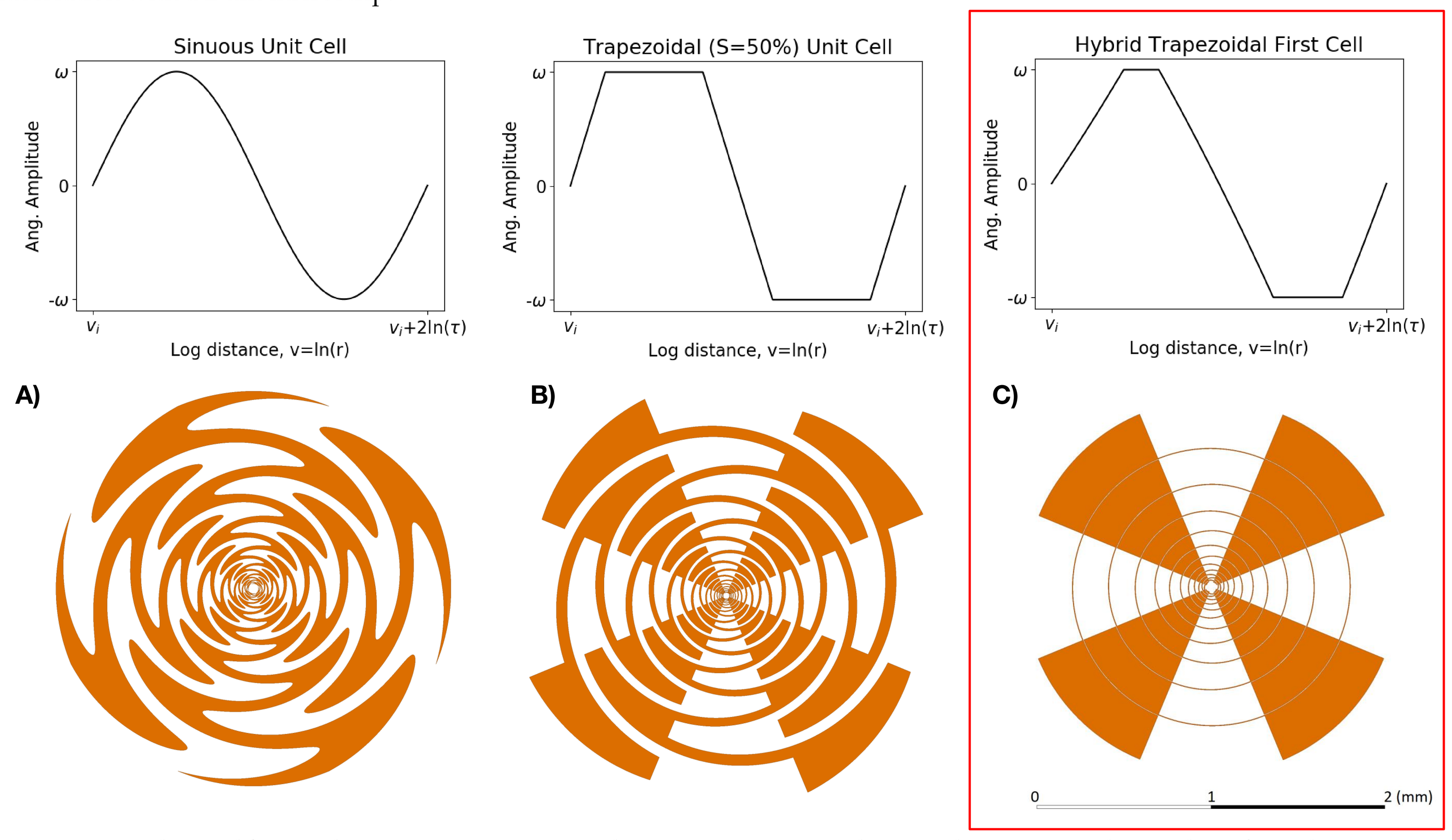

Log-periodic self-similar antennas are other promising planar designs. The side of each arm is defined by a unit cell in radial log-space (Fig. 4 top plots), commonly oscillating between an angular amplitude of ±ω. Then the angular difference between arm sides is δ, with a unit cell expansion rate of τ that characterizes the length of the unit cell. For M unit cells and r_i inner radius, the outer radius can be defined as $r_o = r_i\ \tau^{2M}$.

A four-arm self-complementary layout requires ω = 45° = δ, while $\tau > 1$ can vary. Common examples are the sinuous and trapezoidal patterns (Fig. 4 A & B). The sinuous has been extensively analyzed for other CMB detectors [2], but the trapezoidal has only been used for larger wavelengths. A possible reason is that the narrow portions of the trapezoidal arms become too small to accompany microstrips at small wavelengths.

One solution is to modify the trapezoidal design so the slope S (defined as the % that the unit cell spends at ±ω) varies with radius. In that way, the narrow part of the arm can remain a constant width (in our case, 4 um for a 2 um microstrip). This hybrid trapezoidal is shown in Fig. 4C, no longer log-periodic (but still self-complementary).

Analysis

Simulations of all antennas were done in High Frequency Structure Simulator (HFSS) with microstrips reduced to two simple lumped ports. The initial log-periodic designs were used to reproduce the sinuous results outlined in [2] and compare with the trapezoidal.

Initial Log-Periodic Designs

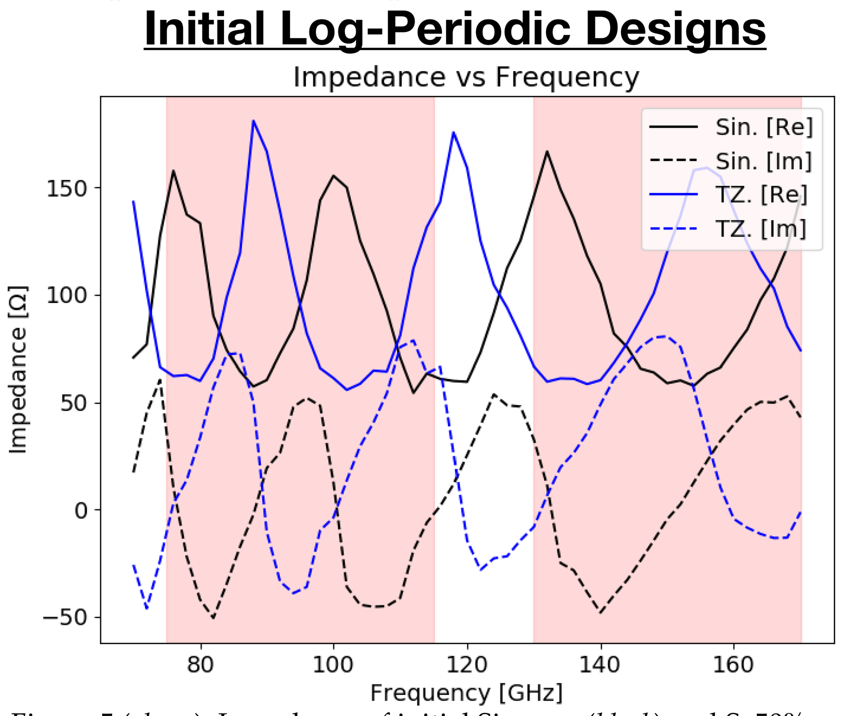

Figure 5 (*above*): Impedance of initial Sinuous (*black*) and S=50% Trapezoidal (*blue*) designs. 95 and 150 GHz bands highlighted. Expected Z value from Eq. 1 becomes 105Ω (due to silicon lenslet), but both fluctuate by ~40%.

Figure 6 (*below*): Polarization wobble (change in expected polarization direction) of both initial designs. Sinuous is within ±5°, while the Trapezoidal is minimally better at ±4°.

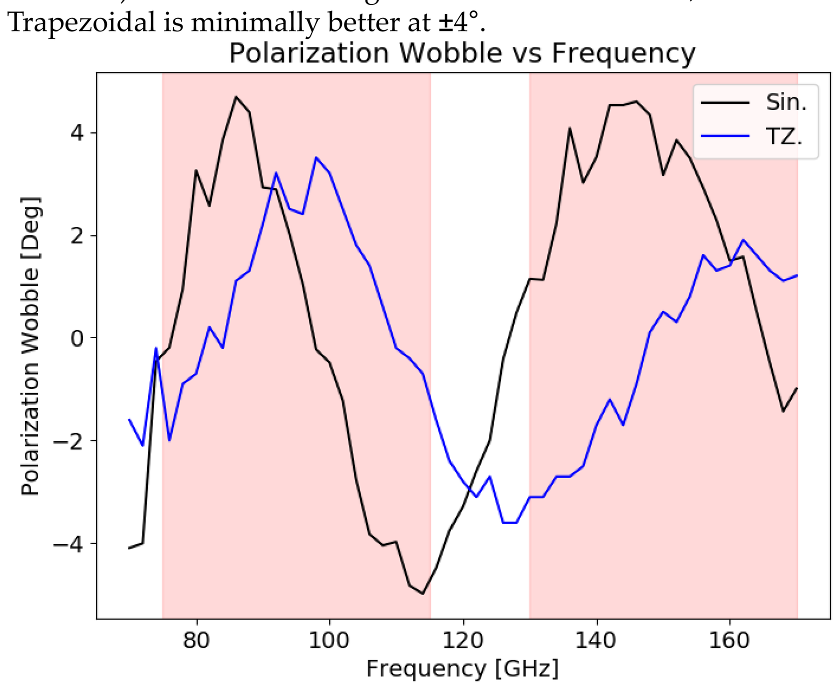

Final Designs: Basic/Bowtie and Hybrid Trapezoidal

Antenna Design	r_i (um)	M	τ	L/R	Beam Efficiency		Ellipticity (a-b)/(a+b)		Max. X-Pol
					150 GHz	220 GHz	150 GHz	220 GHz	
Bowtie	10.0	9	1.30	0.38	55.7%	45.4%	0.008	0.087	5%
Hybrid TZ.	29.8	6	1.35	0.42	85.5%	88.0%	0.017	0.045	2%

Table 1 (*above*): Final design parameters and simulated HFSS beam characteristics. L/R refers to the ratio of lenslet dimensions. Beam efficiency and ellipticity were calculated from normalized beam patterns, while the cross-polarization (X-Pol) is the percentage of normalized gain orthogonal to the desired polarization.

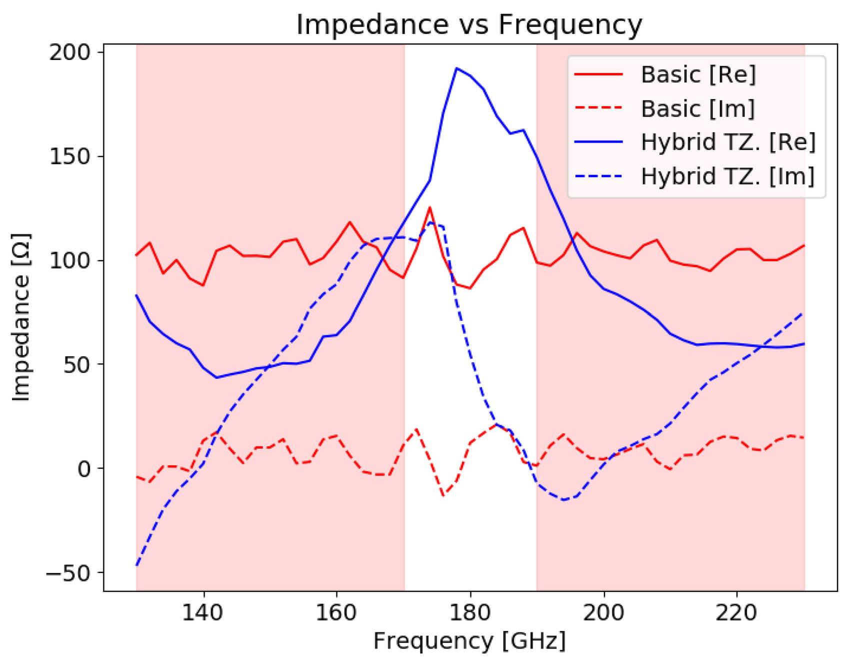

Figure 7 (*above*): Impedance of final Basic/Bowtie (*red*) and Hybrid Trapezoidal (*blue*) designs. Expected Z value from Eq. 1 becomes 105Ω (due to silicon lenslet). The Hybrid Trapezoidal peak was positioned between the desired 150 and 220 GHz bands.

Figure 8 (*below*): Polarization wobble of final designs. Basic/Bowtie has small ±0.2° variations, while the Hybrid Trapezoidal is ±5°.

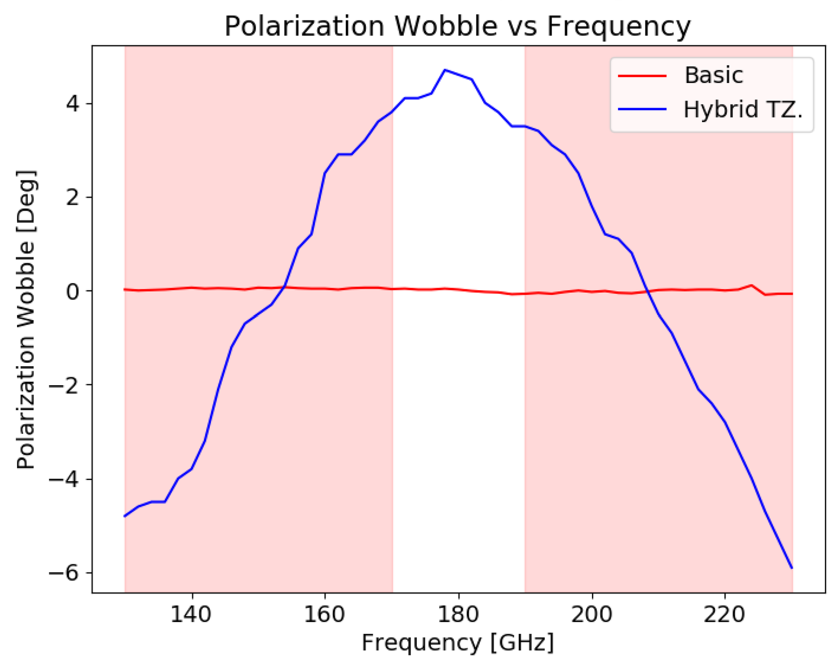

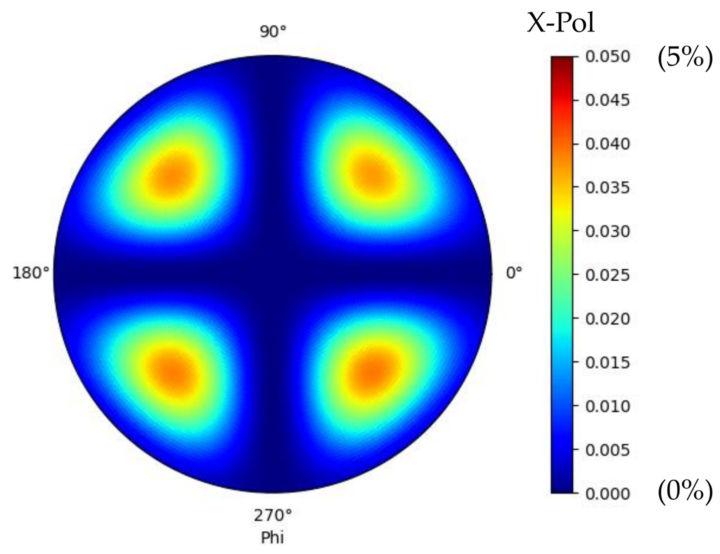

Figure 9 (*above*): Top-down view of cross-polarization gain pattern for Basic/Bowtie design at 220 GHz, for $0° < \theta < 30°$.

Figure 10 (*below*): Top-down cross-polarization gain pattern for Hybrid Trapezoidal design at 220 GHz, for $0° < \theta < 30°$.

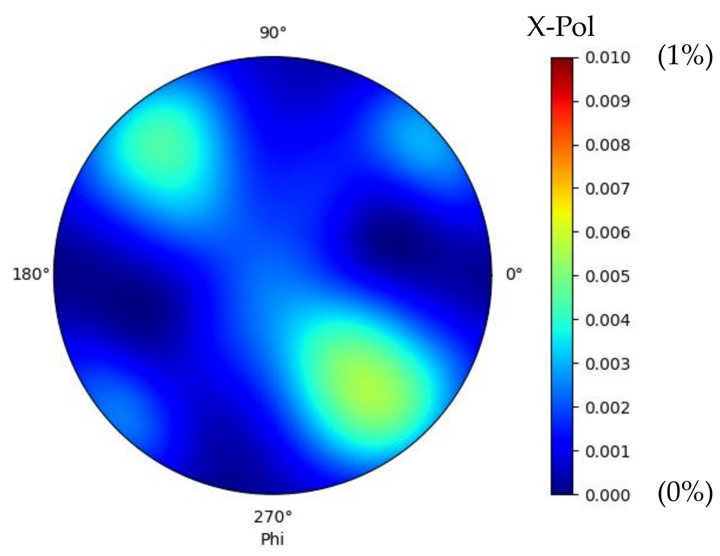

Future Work

Both of the final antennas carry benefits. The basic bowtie offers accurate polarimetry for instances where efficiency is not a big concern, while the hybrid trapezoidal provides stronger detection with a more complex polarization readout.

Only preliminary fabricated test arrays have been made. The arrays consist of the antenna pattern cut out of a ground plane on a silicon wafer, coupled via microstrip (hybrid trapezoidal in Fig. 11) with multichroic Microwave Kinetic Inductance Detectors (MKIDs) which are multiplexed and read out from a single transmission line[3]. The AR-coated lenses are deposited onto the silicon side, simplifying array mount designs.

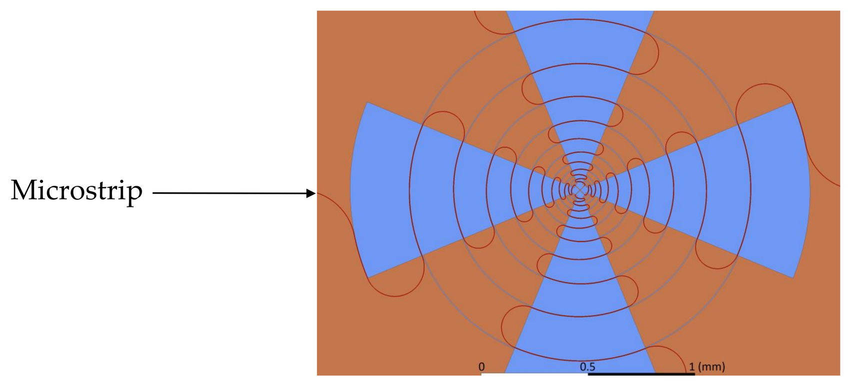

Figure 11: Close-up HFSS diagram of the hybrid trapezoidal cut out of the ground plane, with the microstrips (*red, labeled*) winding down the arms towards the center cross-feed. Similar to Fig. 2.

Acknowledgements

This work is supported by NSF Grants AST-1509211 and AST-1711160 for Johnson; AST-1509078 and AST-1711242 for Mauskopf; AST-1506074 and AST-1710624 for Irwin. We also thank Dr. A. Suzuki (UC Berkeley) for his HFSS sinuous design, used in our initial comparison.

ASU Department of Physics
Arizona State University

References:

[1] G. A. DeSchamps, *IRE Trans. Antennas Propag.* 7, 5, (1959), DOI:10.1109/TAP.1959.1144717.

[2] A. Suzuki, PhD Thesis, University of California, Berkeley (2013).

[3] B. R. Johnson, D. Flanigan, M. H. Abitbol, P. A. R. Ade, S. Bryan, H.-M. Cho, R. Datta, P. Day, S. Doyle, K. Irwin, G. Jones, D. Li, P. Mauskopf, H. McCarrick, J. McMahon, A. Miller, G. Pisano, Y. Song, H. Surdi, and C. Tucker, *J. Low Temp. Phys.* 193, 103, (2018), DOI:10.1007/s10909-018-2032-y.

22-26 JULY 2019 MILANO
LTD 18
LOW TEMPERATURE DETECTORS